2 Petrological Framework

2.1 Magmatic Fractionation

As a consequence of its generally incompatible behaviour shown above, tin becomes enriched in the most fractionated parts of the Earth's crust, i.e. in granitic rocks. The magmatic process of tin enrichment follows, to a first approximation, the law of fractional crystallization (Rayleigh equation). This gives element distribution patterns distinctly different of postmagmatic-hydrothermal tin patterns (Groves 1972; Groves and McCarthy 1978; Boissavy-Vinau and Roger 1980; Lehmann 1982; Higgins et al. 1985; Schermerhorn 1987; Tischendorf 1988). Fractional crystallization in petrology is historically associated with the physical idea of gravitational crystal settling, which, however, need not occur in order for fractional crystallization to proceed. Natural exposures of granitic rocks as well as experimental studies suggest a fluid-dynamically controlled, convective crystal-liquid separation process in the sense of convective fractionation (Rice 1981; Sparks et al. 1984) in which fractionation is due to convection of fluid away from crystals, as opposed to sinking or floating of crystals away from the melt.

Fractional crystallization in evolved granitic rocks results in systematic enrichment and depletion patterns of Ca, Mg, Fe, Ti and many trace elements with only little variation of Si, Al, K and Na. These trends are interpreted to result from sequential crystallization of granitic rock components near the cotectic of the Qz-Ab-Or-An-H_2O system. The conventional reasoning runs along the line that fractionation of mafic minerals, particularly biotite and magnetite, leads to depletion of the residual melt in Fe, Mg, Ti, Co, Ni, Cr, etc.; fractionation of plagioclase results in depletion of Ca, Sr, Eu; fractionation of K-feldspar depletes the residual melt in Ba and Sr; fractionation of the accessory minerals monazite, allanite and titanite depletes LREE in coexisting melt, whereas zircon depletes HREE. Larger, highly charged cations like Sn^{4+}, W^{6+}, Ta^{5+}, U^{4+}, Mo^{6+}, very large cations like Cs^{1+}, Rb^{1+}, as well as small variably charged cations like Be^{2+}, B^{3+}, Li^{+}, P^{5+}, are incompatible with the major silicate phases (structural constraints) and become enriched in residual liquids.

An alternative explanation for such fractionation trends was advanced in studies on the Bishop Tuff by Hildreth (1979, 1981), emphasizing a process of thermogravitational diffusion. Liquid-liquid fractionation by diffusion of melt

components in a thermal gradient (Soret effect) is, however, not compatible with some element relations in fractionation series, particularly with REE patterns (Miller and Mittlefehldt 1984). Evidence for fractional crystallization in the Bishop Tuff has been presented by Michael (1983) and Cameron (1984). Liquid-liquid fractionation is also a process difficult to conceive as an enrichment process for heavy metals such as Sn, Mo and W, which even in simple complexes are relatively heavy with respect to silicate melt compounds. The reduced degree of polymerization in highly fractionated granite melts (i.e. melts rich in H_2O, F and B) would further reduce differences in molecular weights between metal and silicate melt components. Field relations often identify the most fractionated granite phases as being related to small and late-stage subintrusions peripheral to large batholiths, and not limited just to diffuse apical portions of large intrusions, as implied by a thermogravitational model.

This situation can be explained by a model of solidification of large magma chambers from the margins inwards, i.e. sidewall crystallization (McCarthy and Groves 1979; Miller and Mittlefehldt 1984). The relatively cold walls of magma chambers are the most likely place for crystallization to occur. Crystallization on the walls may create a boundary layer of more siliceous and less dense melt which can rise along the edges of the magma chamber, and collect at the top of the system in the form of highly fractionated subintrusions. There must be a transition zone between the largely liquid convecting magma chamber interior and the solid enclosing rock, and the fact of magmatic differentiation points to an efficient crystal-liquid separation process in such a zone. This implies that part of the residual liquid from the crystallizing margins of a magma chamber remains trapped as intercumulus melt whereas another part must return to the interior melt portion. A quantification of such an in-situ crystallization model has been proposed by Langmuir (1989). The consequence of this model is a modification of the ($\overline{D}$ i-1) exponent in the Rayleigh equation of fractional crystallization (see below) by a dynamic term dependent on both bulk distribution coefficient $\overline{D}$ i and the rate of recycled/trapped liquid in the solidification zone, which in turn depends on the physical nature of the individual solidification situation. The complexity of the envisioned crystal-melt separation process during magmatic evolution makes a quantitative modelling on the basis of perfect or equilibrium fractional crystallization questionable (assuming closed or periodically replenished magma chambers). There is the additional complication that there will always be some degree of interaction between the melt system and its wall rocks. The process of combined wall-rock assimilation and fractional crystallization, which is most important for lower

crustal environments with a small thermal gradient between magma and its country rocks, has been modelled by DePaolo (1981).

2.2 Geochemical Heritage

The province-bound character of tin deposits and their temporally repetitive nature in some tin provinces (",tagement temporel"; Routhier 1967) provides the basis of the concept of geochemical heritage of tin. A well-known example is the Bolivian tin province, where Precambrian tin mineralization has been thought to be regenerated by Permo-Triassic and Tertiary magmatism (Stoll 1964; Schuiling 1967; Fleischer and Routhier 1970; Schneider and Lehmann 1977). Apparently Proterozoic tin concentrations have been discussed in the Erzgebirge as source of the later Permo-Carboniferous tin mineralization (Baumann 1965; Weinhold 1977). The South China tin province is discussed in terms of a variety of metallogenetic models of heritage which propose synsedimentary tin and tungsten preenrichment from Precambrian up to Devonian times (Liu Yingjun et al. 1984; Cheng Xianyao et al. 1984; Tanelli and Lattanzi 1985; Pei Rongfu and Mao Jingwen 1988).

There is general agreement that granites in association with tin deposits are enriched in a suite of lithophile elements, i.e. elements which are incompatible with the major mineral components during main-stage crystallization. This geochemical specialization can be a result of fractional crystallization, which seems, however, not unequivocally convincing in explaining the tin specialization of tin granites and the existence of tin provinces. Magmatic fractionation is often seen as of minor importance compared to speculative primary tin enrichment in the source material of tin granites or of their wall rocks. Such a model sees the formation of tin granites as a consequence of pregranitic tin enrichments or of regional geochemical tin anomalies (Schuiling 1967; Routhier 1980; Hutchison 1983; and many others).

Geochemical data from granitic fractionation suites allow estimation of both the contribution by pregranitic tin input and the process of intragranitic tin accumulation (Lehmann 1982, 1987). The concept is based on the definition of the partition coefficient D_i

$$\overline{D}_i = X_i(\text{crystals})/X_i(\text{melt}), \qquad (1)$$

where X_i(crystals) and X_i(melt) correspond to the concentration of trace element i in the solid phases (weighted sum of all crystals) in equilibrium with

the melt (Neumann et al. 1954). $\overline{D}_i$ is dependent on pressure, temperature and chemical composition of the system.

A melt with total mass M and partial mass mi of element i develops through crystallization at time t+dt into a residual melt with total mass M-dM and m_i-dm_i, plus a solid mass portion with dM and dm_i. From Eq. (1) follows:

$$dm_i/dM = \overline{D}_i \cdot (m_i-dm_i)/(M-dM) \quad (2)$$

with $dm_i/dM = X_i$(crystals) and $(m_i-dm_i)/(M-dM) = X_i$(melt).

With dm_i and dM very small compared to m_i and M, Eq. (2) simplifies to:

$$dm_i/dM = \overline{D}_i \cdot (m_i/M). \quad (3)$$

Given a crystallization process which prevents continuous reequilibration between solid phases and the melt (slow diffusion in crystal phases, mechanical crystal-melt separation) the recasted Eq. (3)

$$dm_i/m_i = \overline{D}_i \cdot (dM/M) \quad (4)$$

can be integrated between m(0) and m(t) and between M(0) and M(t) to yield:

$$\log [m_i(t)/m_i(0)] = \overline{D}_i \cdot \log[M(t)/M(0)] \quad (5)$$

or

$$m_i(t)/m_i(0) = [M(t)/M(0)]^{\overline{D}_i} \quad (6)$$

Multiplying both sides of Eq. (6) by M(0)/M(t) gives:

$$[m_i(t) \cdot M(0)]/[m_i(0) \cdot M(t)] = [M(t)/M(0)]^{\overline{D}_i - 1} \quad (7)$$

and

$$X_i(t) = Xi(0)\ [M(t)/M(0)]^{\overline{D}_i - 1} \quad (8)$$

The ratio M(t)/M(0) is the fraction of original melt remaining, F, or degree of fractionation:

$$c_i(t) = c_i(0) \cdot F^{\overline{D}_i - 1} \quad (9)$$

This is the standard equation for all perfect fractional crystallization or distillation processes, known as the Rayleigh fractionation law (Rayleigh 1896; Doerner and Hoskins 1925).

The validity of this relationship for specific sample populations can be examined by log-log variation diagrams of two trace elements i and j, in which linear correlation indicates fractional crystallization. This results from:

$$\log [X_i(t)/c_i(0)] = [\overline{D}_i - 1] \cdot \log F \quad (10)$$

$$\log [X_j(t)/c_j(0)] = [\overline{D}_j - 1] \cdot \log F. \quad (11)$$

Equations (10) and (11) combine into:

$$\log [X_i(t)/X_i(0)]/\log [X_j(t)/X_j(0)] = [\overline{D}_i\text{-}1]/[\overline{D}_j\text{-}1] = c. \quad (12)$$

The constant c corresponds to the slope m of the general linear equation of a straight correlation line with the parameters:

$$\log X_i(t) = m \log X_j(t) + b. \quad (13)$$

The term b defines the position of the straight line in a log-log plane and can be used as a relative measure of geochemical heritage with respect to any reference system. This is possible by plotting data pairs of a neutral indicator of magmatic fractionation i (such as Ti, Rb/Sr, Zr, Nb, etc.) against element j which is to be tested for primary geochemical specialization. The graphic model of this concept is shown in Fig. 6.

The above theoretical treatment is based on perfect fractional crystallization, i.e. perfect and continuous separation of solid phases and melt. This situation is not realized under natural conditions because there will always be trapped intercumulus liquid in between crystal phases (Langmuir 1989), and because some of the fractionating liquid will move away from the system (Cann 1982). The theoretical model can nevertheless be applied to natural situations because variable amounts of intercumulus liquid modify the degree of enrichment or depletion, but do not change the general log-log evolution pattern (McCarthy and Hasty 1976; Langmuir 1989).

2.3 Crystal-Melt Partitioning of Tin

The main tin carriers in granitic rocks are biotite, hornblende, titanite, ilmenite and magnetite (Barsukov 1957; Petrova and Legeydo 1965; Rub 1968; Tischendorf 1970; Lange et al. 1972). Preferential substitution of the major cations Ti^{4+} and Fe^{3+} by Sn^{4+} is understandable from the similar crystal-chemical parameters of these components [ionic radii (Å) for coordination number VI: Ti^{4+} 0.61, Fe^{3+} 0.55/0.65, Sn^{4+} 0.69; Shannon (1976)]. This explains also the occasionally high tin contents in intramagmatic titanomagnetite ore deposits (105 g SnO_2/mt ore in Grängesberg, Sweden; Schröcke and Weiner 1981:439).

Tin contents of quartz and feldspars reach up to a few ppm, and are always well below the whole-rock tin content. Granitic differentiation suites with little variation in modal composition give linear correlation trends between tin in bulk rock and tin content in individual mineral phases (Rub 1968; Tischendorf

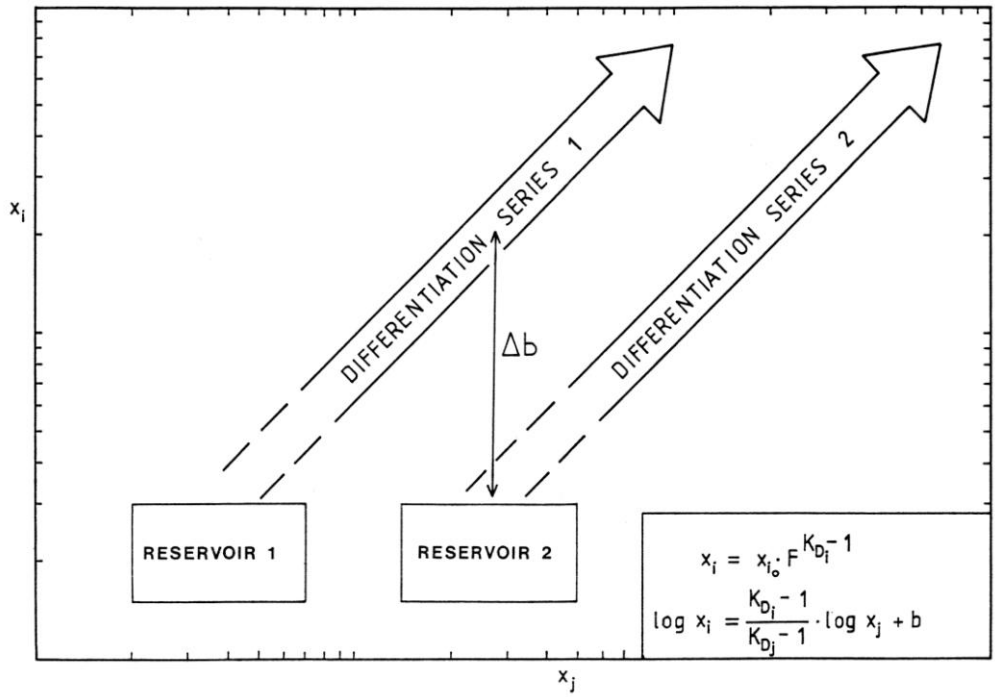

Fig. 6. Quantitative interpretation scheme for geochemical heritage in magmatic fractionation suites. X_i neutral indicator of degree of fractionation; X_j element to be tested for geochemical heritage, i.e. input from geochemically anomalous source

1970; Lange et al. 1972). An example of the relation Sn (biotite)-Sn (whole rock) from the Erzgebirge granites is given in Fig. 7.

A quantitative measure of these distribution trends is given by the tin distribution coefficient DSn, which in its simplest form and for trace concentrations XSn can be defined from expression (1) as

$$D_{Sn} = X_{Sn}(\text{crystal})/X_{Sn}(\text{melt}) \quad (14)$$

The bulk tin distribution coefficient DSn for the whole rock is then

$$\overline{D}_{Sn} = [X_{Sn}(i) \cdot M_i/M + X_{Sn}(j) \cdot M_j/M + \ldots X_{Sn}(n) \cdot Mn/M]/X_{Sn}(\text{melt}) \quad (15)$$

where i, j, ...n are individual mineral phases with mass M_i, M_j, ...M_n of the total mass M of all solid phases.

This definition of the distribution coefficient does not take into account the temporal evolution of crystallization and the resulting heterogeneous element distribution within individual crystal phases. The commonly adopted method

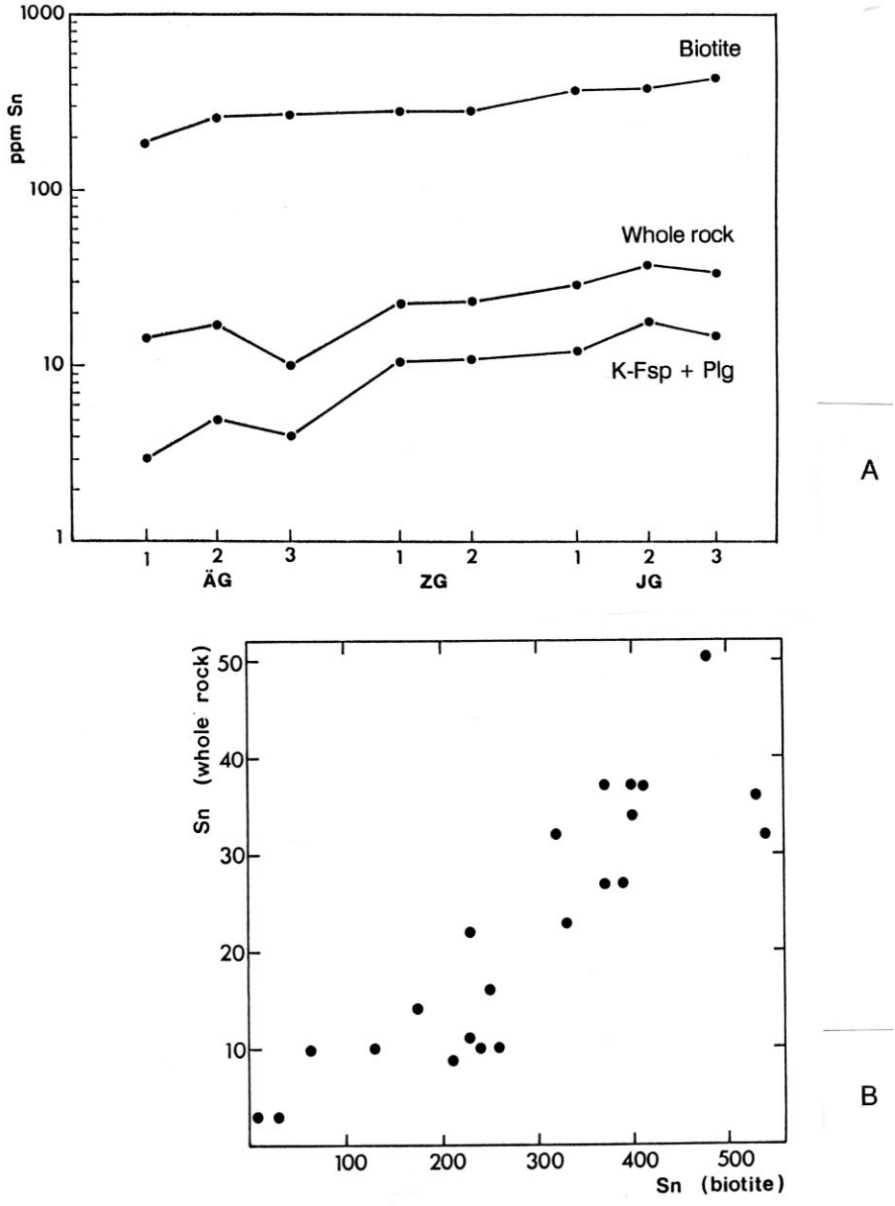

Fig. 7. A The distribution of tin in feldspars (K-feldspar + plagioclase), biotite and whole rock for individual granite phases of the western Erzgebirge batholith. **ÄG** Ältere Granite (Older Granites); **ZG** Zwischengranite (Transitional Granites); **JG** Jüngere Granite (Younger Granites).
B The correlation of tin content in whole rock and in biotite in granite samples from the Erzgebirge and the Thuringian Forest. Data from Bräuer (1970), Tischendorf (1970), Lange et al. (1972)

of empirical determination of distribution coefficients by comparing element contents in phenocrysts and their matrix is therefore only a rough approximation.

Empirical tin distribution coefficients determined by this latter method for quartz, K-feldspar, plagioclase, clinopyroxene, olivine, biotite, muscovite and magnetite in various volcanic and subvolcanic rocks of basaltic to rhyolitic composition are compiled in Fig. 8 according to Kovalenko et al. (1988). The data are mean values from a large data base; temperature estimates are derived from petrological equilibria. The corresponding data for tungsten, which give less pronounced trends than for tin, are included in Fig. 8 for comparison. Distribution coefficients for titanite were not measured by Kovalenko et al. (1988). Data from Petrova and Legeydo (1965) suggest for titanite a tin distribution coefficient approximately ten times larger than for magnetite.

The T-D_{Sn} systematics of Fig. 8 allows some conclusions on the behaviour of tin during melt formation. Partial melts with T ≥1000°C, i.e. the temperature conditions relevant to melting of mantle material, cannot be rich in tin because such melts are in equilibrium with olivine and/or pyroxene with both extremely low tin contents of less than 1 ppm (Hamaguchi and Kuroda 1969) and D_{Sn} ≈1. The calc-alkaline evolution path of andesitic melts seems to be related to fractionation of magnetite (Gill 1978; Osborn 1979) and will therefore produce tin depletion in the melt. The formation of alkali-rich melts by breakdown of biotite/phlogopite at a low degree of melting is equally a process which at high temperature and correspondingly D_{Sn} ≈1 will not give substantial tin enrichment in the melt fraction relative to the source material. The likely fractionation of magnetite during the calcalkaline magmatic evolution will, in addition, produce a drastic reduction of the tin level of primitive melts.

Granitic melt formation and evolution in an intracrustal environment provides a different situation. The relatively low melt temperature and the correspondingly small tin distribution coefficient for the main mineral components plagioclase, K-feldspar and quartz lead to tin enrichment in the melt phase, an effect partially offset by mafic liquidus phases with D_{Sn}(xtl/melt) >1, such as biotite, muscovite, accessory Fe-Ti phases. Muscovite is, however, unstable in fractionating, high-level magma chambers (≤1.5 kbar), even at high B and F levels, and must be considered as of sub-solidus formation (Manning and Pichavant 1984). The small DSn of quartz will lead to tin enrichment particularly in low-temperature, volatile-rich granite systems near the thermal minimum in which feldspars + quartz co-crystallize.

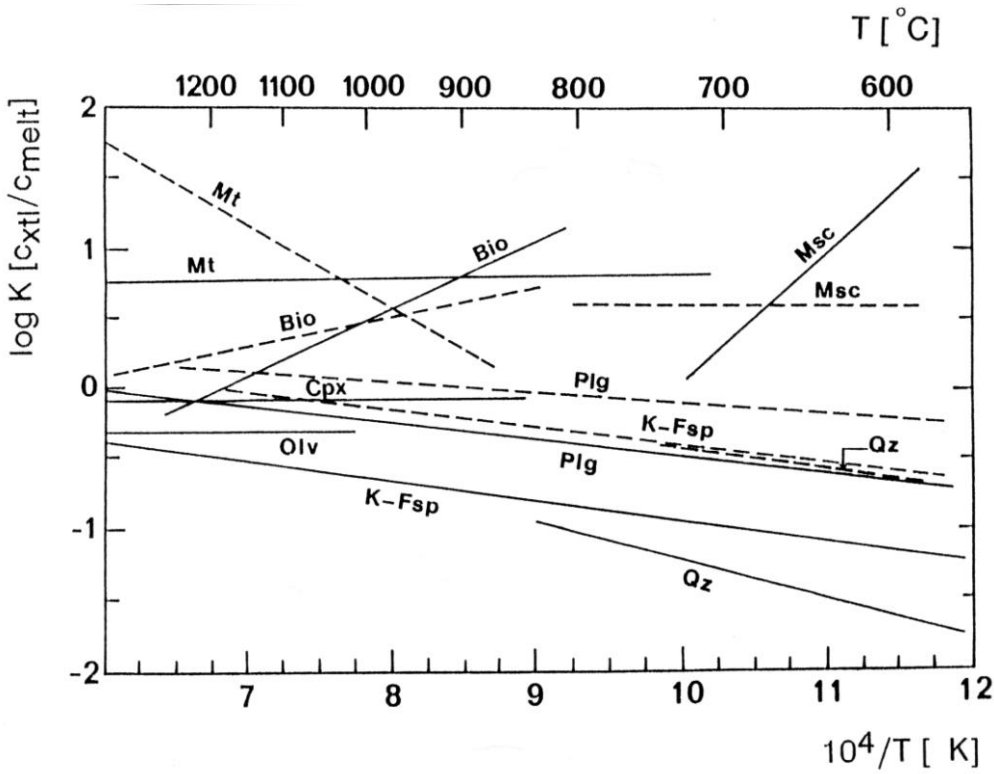

Fig. 8. Tin and tungsten distribution coefficients of magnetite (Mt), biotite (Bt), muscovite (Msc), olivine (Olv), clinopyroxene (Cpx), plagioclase (Plg), K-feldspar (K-fsp), quartz (Qz) as a function of temperature in volcanic/ subvolcanic rocks of basaltic to rhyolitic composition. Solid lines are for tin, broken lines for tungsten. Data from Kovalenko et al. (1988)

The bulk tin evolution trend in granitic melts will depend on the proportion of leucocratic/femic minerals. Because the femic minerals crystallize predominantly during relatively early stages of melt evolution, the bulk tin distribution coefficient can be expected to decrease during melt evolution. The increasing degree of fractionation leads to increasing levels of volatile components which have a depolymerizing effect on melt structure. This allows a more efficient fractional crystallization process through lowered melt viscosity (Burnham 1979b) and, in addition, may shift DSn(xtls/melt) towards smaller values. Granitic melts can essentially be considered as a mixture of an aluminosilicate polyanionic (network-forming) framework and an interstitial cationic (network-modifying) component. The aluminosilicate structural units form a three-dimensional network composed of polymerized $[AlSi_3O_8^-]_n$ $[Si_4O_8^0]_m$ units charge-balanced by interstitial cations. The principal

depolymerizing components in granitic melts are, besides the ferromagnesian cations (which are drastically reduced during fractional crystallization), alkalies or aluminum in excess of the amount required to charge-balance the alkali-aluminosilicate tetrahedra (i.e. peralkaline or peraluminous melts), as well as anionic depolymerizers of which OH^- and F^- are the most effective (Dingwell 1988). The strongly viscosity-reducing effect of water and fluorine will accelerate crystal-liquid fractionation, extend the temperature range of crystallization, and increase melt component diffusivities, i.e. possible diffusive fractionation mechanisms such as Soret or thermogravitative fractionation (Burnham 1979b; Dingwell 1988). There is evidence that Al^{3+} behaves like a network-modifying cation in peraluminous melts promoting depolymerization of the melt and lowering of the liquidus temperature (Mysen et al. 1985).

Tetravalent tin in silicate melts has probably octahedral coordination with oxygen and is copolymerized with the aluminosilicate network through Sn-O-Si bonds (Stemprok 1989). Increasing concentrations of anionic ligands in the melt which can serve as complexing agents for tin will favour lower crystal/melt partition coefficients. Chloride, fluoride, and hydroxyl strongly complex tin in aqueous solutions. If this relationship holds for silicate melts, an increase of these ligands during fractional crystallization could account for the observed relationship in some rhyolites which show an inverse proportionality between D_{Sn}(xtl/melt) and whole-rock tin content, i.e. degree of fractionation (Antipin et al. 1981; Kovalenko et al. 1984). The mineral-melt distribution coefficients for tungsten have similar characteristics like those of tin (Fig. 8); both temperature and compositional variability are, however, less pronounced than in the case of tin.

Mahood and Hildreth (1983) demonstrated that crystal-liquid partition coefficients in silicic melts can change widely in response to change in melt structure. Urabe (1985) suggested that the alkali/alumina ratio is a major factor controlling activity coefficients of cations in aluminosilicate melts and controlling the metal concentration in released magmatic fluids. Peraluminous melt composition seems to be a precondition for efficient release of chlorine-complexed metals. Partition coefficients are dependent on a variety of melt parameters which are probably not yet all identified, and the presently available specific data allow only qualitative generalizations.

2.4 The Role of Oxidation State

Ishihara (1977) observed two different distribution patterns of accessory opaque minerals in Japanese granitic rocks: a granite population with magnetite, ilmenite, hematite, pyrite and titanite (sphene); and a second granite population with no magnetite and titanite, but with ilmenite, pyrrhotite and ± graphite. Both general granite groups are defined as magnetite- and ilmenite-series, respectively (Ishihara 1977), and differ from each other also by magnetic susceptibility and Fe_2O_3/FeO ratio (both parameters are greater in magnetite-series rocks) (Takahashi et al. 1980; Ishihara 1981). Copper and molybdenum porphyries are part of the magnetite-series granitic rocks, whereas tin granites and porphyries are part of the ilmenite-series granite spectrum (Ishihara 1981).

The different opaque mineral association and Fe_2O_3/FeO ratios in both granite series can be interpreted to reflect different oxygen fugacity during the formation of these rocks, i.e. during their magmatic and subsequent history. Some important oxygen buffers are shown in Fig. 9 as a function of oxygen fugacity and temperature. The separation line of magnetite- and ilmenite-series granitic rocks must be located between the petrogenetic buffer systems hematite-magnetite and quartz-magnetite-fayalite, more specifically near the equilibrium pyrite + magnetite + pyrrhotite and the lower stability limit of the assemblage titanite + magnetite + quartz. The reaction

$$3CaTiSiO_5 + 2Fe_3O_4 + 3SiO_2 = 3CaFeSi_2O_6 + 3FeTiO_3 + O_2 \qquad (16)$$

titanite + magnetite + quartz hedenbergite + ilmenite

has been calibrated by Wones (1989). The equilibrium expression is

$$\log f O_2 = -30930/T + 14.98 + 0.142(P-1)/T \qquad (17)$$

where T is the temperature (in K) and P is the pressure (in bar). The equilibrium is affected by impurities in natural occurrences of the above mineral phases. The effect of dilution of the $FeTiO_3$ component by solid solution will be partly offset by solid solution in the magnetite and titanite components (Wones 1989). Natural clinopyroxene-bearing mineral assemblages in granitic rocks will not consist of pure hedenbergite. The effect of a lowered activity of hedenbergite by a greater diopside component is given in Fig. 9. The calculated equilibria correlate with fO_2 reconstructions from the independent Fe-Ti-oxide oxygen geobarometer (see data from Lipman 1971, in Wones 1989).

It is difficult to establish the original oxygen fugacity of a granitic magma from the study of a granite. Slow sub-solidus cooling results in oxidation-exsolution

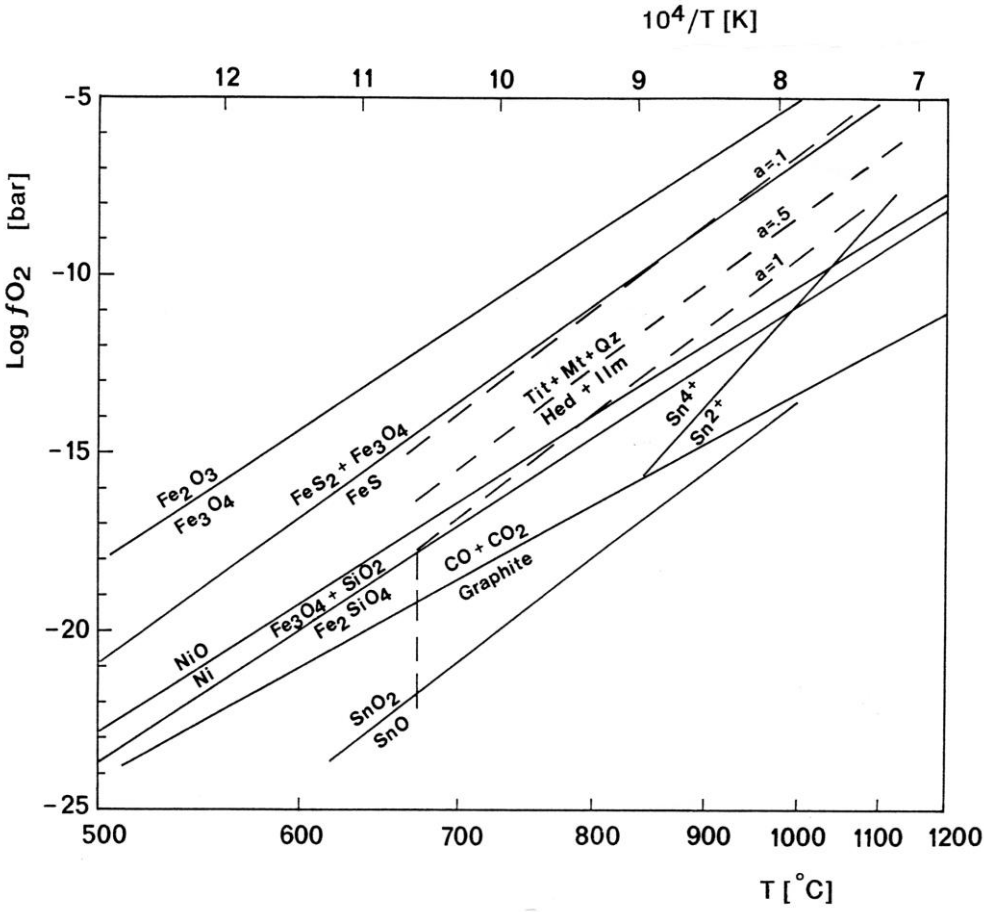

Fig. 9. Some mineral equilibria as function of oxygen fugacity fO_2 and temperature T. Broken lines labelled a = 1, 0.5 and 0.1 depict shift in equilibrium of the assemblage titanite-magnetite-quartz-hedenbergite-ilmenite as a result of lowered activity a of hedenbergite (greater diopside component) in clinopyroxene. Magnetite-series granitic rocks are located between and above the titanite-magnetite-quartz-hedenbergite-ilmenite and pyrite-magnetite-pyrrhotite buffer lines. Ilmenite-series granitic rocks are located below this region with a lower limit at the graphite-CO-CO_2 buffer. See text for discussion of Sn^{4+}/Sn^{2+} and SnO_2/SnO equilibrium. Data sources: fayalite-quartz-magnetite from Hewitt (1978), Ni-NiO from Huebner and Sato (1970), hematite-magnetite from Eugster and Wones (1962), graphite-CO+CO_2 at 1 kbar from French and Eugster (1965), titanite-magnetite-quartz-hedenbergite-ilmenite from Wones (1989), SnO_2-SnO from thermodynamic data in Hirschwald et al. (1957), Sn^{4+}-Sn^{2+} in sodium silicate from Johnston (1965)

of Fe-Ti oxides which severely limits the application of such phases as an oxygen geobarometer. The recognition of the primary mineral assemblage titanite + magnetite versus clinopyroxene (or amphibole) + ilmenite can therefore be an important aid in reconstructing the relative oxidation state in a melt.

There is also the possibility of inferring the oxidation state of a melt directly from the Fe_2O_3/FeO ratio of the resultant rock. The iron oxidation reaction in silicate melts is commonly expressed in terms of the reaction

$$2FeO + ½O_2 = Fe_2O_3. \quad (18)$$

Experimental data on quenched silicate melts fit an empirical expression of the form (Sack et al. 1980; Kilinc et al. 1983)

$$\ln[XFe_2O_3/XFeO] = a\ln f O_2 + b/T + c + \Sigma d_i X_i, \quad (19)$$

where a,b,c and d are regression coefficients and the sum is over the oxide components i. More recent experimental data from Kress and Carmichael (1988) and Mysen and Virgo (1989) confirm that $\ln[XFe_2O_3/XFeO]$ is a linear function of $\ln f O_2$ and 1/T over a wide range of oxygen fugacities and melt compositions, and that coefficient a in Eq. (19) is 0.21, which leads to the refined iron oxidation reaction (Wones 1988)

$$FeO + 0.232\ O_2 = FeO_{1.464}. \quad (20)$$

The activity coefficients of the components in Eq. (18) are strongly dependent on melt composition and structure, particularly on the Al/Al+Si ratio and on the NBO/T parameter (non-bridging oxygens per tetrahedrally coordinated cation), which led Mysen and Virgo (1989) to a further refinement of Eq. (19). Given a similar temperature range of crystallization and similar melt composition, $\log[Fe^{3+}/Fe^{2+}]$ ratios in granitic rocks can, however, used as a simplistic approximation of the magmatic $\log fO_2$ conditions. It is assumed that with limited water/rock interaction a rock-buffered external fluid phase will not change significantly the Fe_2O_3/FeO ratio in the rock.

The empirical application of this concept is given in Fig. 10 in which Fe_2O_3/FeO ratios of granitic host rocks from three major ore environments (copper porphyries, molybdenum porphyries, tin porphyries/granites) are compared. SiO_2 is used as the most simple expression for the general degree of magmatic differentiation. The limit between magnetite- and ilmenite series granites is empirically derived (Ishihara et al. 1979). The Fe_2O_3/FeO ratio of this dividing line corresponds closely to the idealized molecular ratio Fe_2O_3/FeO = 0.5 for the equilibrium magnetite/ilmenite (assuming no other Fe-bearing phases present).

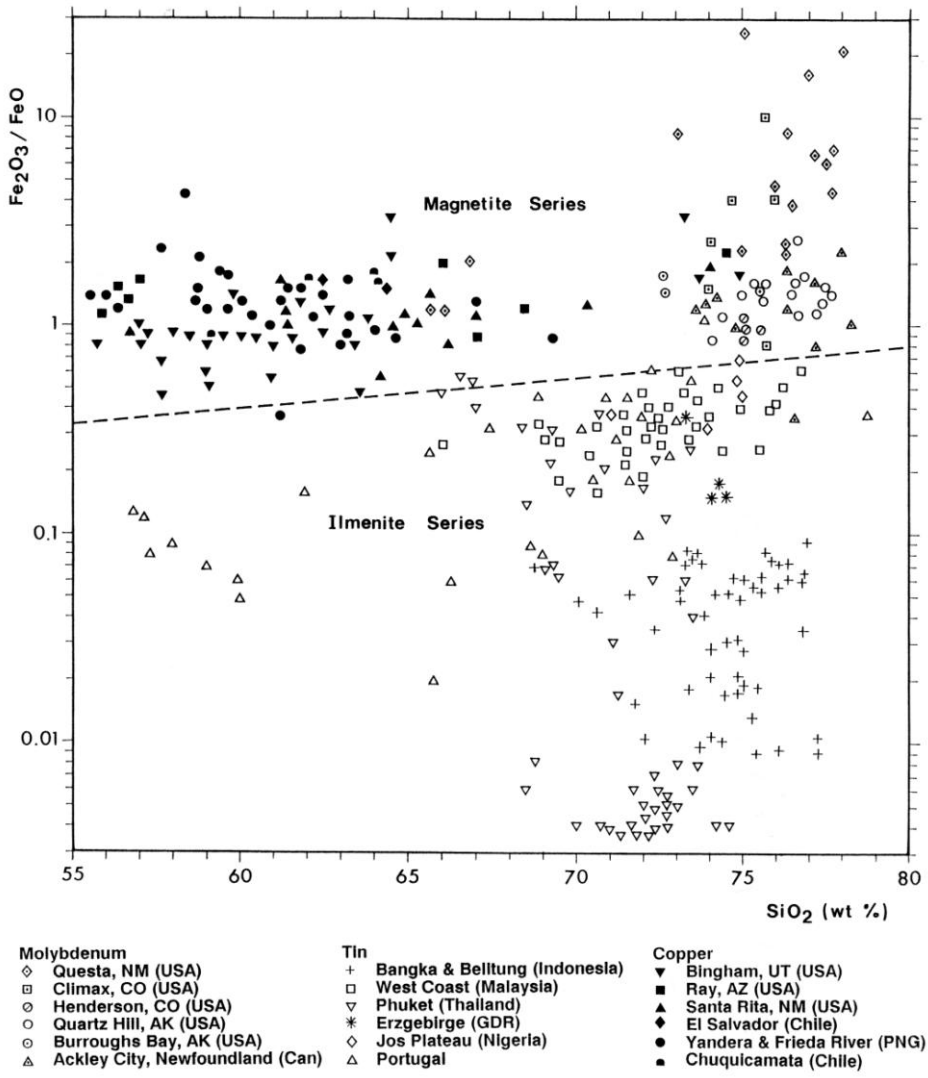

Fig. 10. SiO_2-Fe_2O_3/FeO variation diagram for granitic rocks in association with copper, molybdenum, and tin deposits (copper porphyries, molybdenum porphyries, tin porphyries/granites). The empirical dividing line between ilmenite and magnetite series rocks is for granites in Japan (Ishihara et al. 1979). Rock data compiled from Albuquerque (1971), Banks et al. (1972), Gustafson and Hunt (1975), Hudson et al. (1979, 1981), Imeokparia (1986a), Ishihara (1967), Ishihara et al. (1984), Johnson and Lipman (1988), Jones et al. (1967), Keith (1984), Lange et al. (1972), Lanier et al. (1978), Liew (1983), Mason and McDonald (1978), Moore (1978), Moore et al. (1968), Neiva (1976), Pitfield (1987), Putthapiban (1984), Watmuff (1978), Whalen (1980), Whalen et al. (1982) and White et al. (1981)

The granitic rocks in association with the three major magmatic-hydrothermal ore environments plot in three different fields of the Fe_2O_3/FeO-SiO_2 diagram of Fig. 10. The copper porphyry environment is characterized by relatively little differentiated, magnetite-series granitic rocks. The much more differentiated granitic rocks in association with molybdenum and tin deposits are distinguished from each other by distinctly different oxidation state. Tin granites from the particularly rich tin districts of Phuket (Thailand) and of the Tin Islands (Indonesia) display extremely low Fe_2O_3/FeO ratios.

This general distribution pattern strengthens the assumption that oxygen fugacity plays a critical role in the evolution of these magmatic-hydrothermal systems. Given an effective fractional crystallization process, low $\boldsymbol{f}O_2$ (i.e. ilmenite-series granites) seems to favour the formation of tin ore systems, whereas high $\boldsymbol{f}O_2$ (i.e. magnetite-series granites) seems to favour the formation of molybdenum ore systems. The complementary behaviour of tin and molybdenum is also portrayed in the overall bipolar metal distribution of the Sn-W-Mo ore deposit spectrum, with tungsten having a less pronounced affinity for either ilmenite- or magnetite-series rocks.

The redox pair Sn^{4+}/Sn^{2+} provides an explanation for this pattern (analogous: $Mo^{6+}/Mo^{4+}/Mo^{3+}$). The crystal-chemical properties of both tin species are largely different, with ionic radii of $^{VI}Sn^{4+}$ 0.69 Å and $^{VI}Sn^{2+}$ 0.93 Å (Shannon 1976). Under the assumption that both Sn^{2+} and Sn^{4+} species can be stable in granitic melts, a relationship such as $\overline{D}_{Sn^{4+}}$(xtls/melt) >1 (substitution of Sn^{4+} by Ti^{4+} with ionic radius of 0.61 Å at coordination number VI) and $\overline{D}_{Sn^{2+}}$ <1 is required (Ishihara 1981). The theoretical basis of this concept can be formulated for a melt as

$$O_{2-} + Sn^{4+} = Sn^{2+} + \tfrac{1}{2}O_2, \qquad (21)$$

and similar to the expression in Eq. (19):

$$\ln[Sn^{2+}/Sn^{4+}] = -\tfrac{1}{2}a\ln\boldsymbol{f}O_2 + b/T + c + \Sigma d_i X_i. \qquad (22)$$

Dominance of Sn^{4+} in relatively oxidized melts will result in a bulk tin distribution coefficient $\overline{D}_{Sn}$(xtls/melt) >1, whereas dominance of Sn^{2+} in more reduced melts relates to $\overline{D}_{Sn}$(xtls/melt) <1. The reverse relationship can be formulated for molybdenum.

The thermodynamic background for this argumentation is not well known. The equilibrium SnO-SnO_2 (calculated from data in Hirschwald et al. 1957) is given in the $\boldsymbol{f}O_2$-T diagram of Fig. 9. The relation of these components to polymerized tin complexes is, however, vague. The position of the equilibrium far below the QFM buffer indicates that SnO is stable only under very reducing conditions; a situation which is however realized in some basaltic and rhyolitic

volcanic rocks (Ewart 1981; Kress and Carmichael 1988; Bryndzia et al. 1989). The experimental determination by Johnston (1965) of the Sn^{4+}/Sn^{2+} equilibrium in $Na_2O \cdot 2SiO_2$ glass at temperatures around 1000°C probably provides a better estimate for the speciation of tin in granitic melts. According to these data, divalent tin can be expected to be stable in ilmenite-series granites at a temperature of ≥800°C (Fig. 9). The data by Johnston (1965) are in agreement with experiments on the valency state of tin in basalt liquids at 1200°C which locate the Sn^{4+}/Sn^{2+} equilibrium at log fO_2 -8 bar, with Sn^{4+}/Sn^{2+} = 0.1 at log fO_2 -11, and Sn^{4+}/Sn^{2+} = 10 at log fO_2 -5 (Durasova et al. 1984). The existence of Sn^{2+} together with the quantitatively dominating Sn^{4+} species in synthetic granite-SnO_2 mixtures prepared under air and at 1600°C has been demonstrated by Mössbauer spectroscopy (Sitek et al. 1981).

The experimental investigation of the distribution coefficient of molybdenum between magnetite and silicic melt by Tacker and Candela (1987) confirms the critical role of oxygen fugacity. D_{Mo}(mt/melt) at 800°C and 1 kbar with fO_2 one-half a log unit above the NNO buffer was found to be 0.21 ± 0.08. A decrease in fO_2 to the graphite-methane buffer was accompanied by an increase of D_{Mo}(mt/melt) to 0.52 ± 0.13. The same relationship is also valid for the system ilmenite-melt, and a reverse but more moderate trend under the same experimental conditions was found for tungsten (Candela and Bouton 1990).

Besides the role of oxygen fugacity during magmatic tin enrichment, for which experimental evidence is not yet available, the hydrothermal mobility of tin is crucially controlled by fO_2 (see below). The association of tin deposits with low-fO_2, ilmenite-series granitic rocks is therefore of additional importance because oxygen fugacity in a fluid phase will be buffered by the granitic wall rock in an early stage of a hydrothermal circulation system, i.e. at low fluid-rock ratio.

2.5 Solubility of Cassiterite in Silicic Melts

Experimental data on the solubility of SnO_2 in granitic melts have been recently compiled by Stemprok (1990) and are given in a generalized form in Fig. 11. Ryabchikov et al. (1978) first noted the dependence of tin solubility on oxygen fugacity and found a solubility limit for tin in eutectic mixtures of albite-sanidine-quartz-H_2O at 1.5 kbar and 750°C of 0.4 wt% Sn at the MW

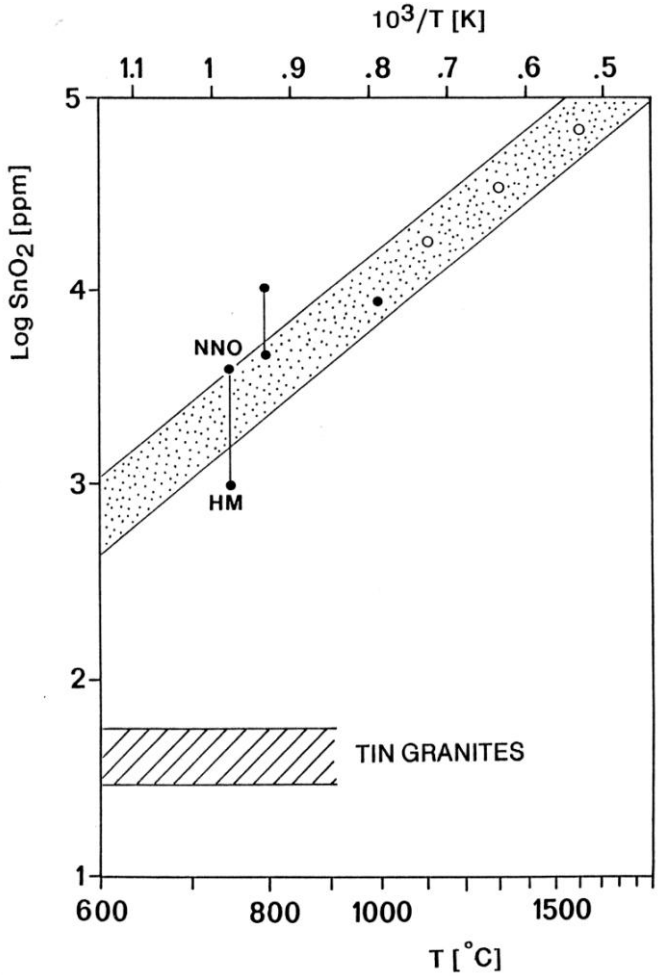

Fig. 11. The experimental solubility of cassiterite in silicic melts as a function of temperature. The stippled trend is from the compilation of Stemprok (1990). Open circles: dry melts at 1 bar and in air; solid dots: melts with excess water at 1.5 kbar and fO_2 between NNO and HM. Data from Ryabchikov et al. (1978) and Stemprok (1990)

buffer, and 0.1-0.2 wt% Sn at the NNO buffer, respectively. These data fit into the general solubility trend for SnO_2 determined at higher temperatures (Fig. 11) and suggest that only in an extremely fractionated environment, i.e. in pegmatites, may a granitic melt become saturated with respect to cassiterite. The average magmatic tin content in tin granites is around 20-30 ppm, much lower than the cassiterite saturation limit. Intramagmatic cassiterite formation is therefore very unlikely even in highly fractionated granites (the often

idiomorphic habit of cassiterite may easily lead to minerogenetic misinterpretations).

The components WO_3 and MoO_3 have solubility characteristics very similar to SnO_2 (Stemprok 1990). Both tungsten and molybdenum oxides have a solubility of °1000 ppm in granitic melts at 750-800°C, which only in exceptional situations allows both molybdenite or wolframite/scheelite to be stable liquidus minerals.

2.6 Melt-Fluid Partitioning of Tin

Volatile-rich granitic melts are able to persist to relatively low magmatic temperatures at high crustal levels. The effect of increasing H_2O content on reducing solidus and liquidus temperatures and on phase relations in the experimental system Qz-Ab-Or-H_2O, i.e. expanding the stability field of quartz with displacement of the thermal minimum composition towards the albite corner, has been shown by the classical studies of Tuttle and Bowen (1958) and Luth et al. (1964). The individual effects of fluorine and boron in the same system are similar to water; however, important only with F or B_2O_3 contents in excess of 1 wt% (Manning 1981; Pichavant 1981; Manning and Pichavant 1984).

The experimentally studied volatiles H_2O, F, B and Li have a - possibly additive - fluxing effect on granitic melts, reducing the temperatures of crystallization. The data show that the addition of F and Li to silicic melts has no effect on the solubility of water at constant pressure (Manning 1981; Martin 1983; Webster 1990), whereas the solubility of water increases with increasing B content (Pichavant 1981), an effect also observed with increasing aluminum content in peraluminous melts (Dingwell et al. 1984). Boron-rich and/or peraluminous melts will therefore reach water saturation at a later stage or at lower total pressure than fluorine-dominated and/or metaluminous melts. Little soluble volatiles such as CO_2 or CH_4 will, on the other hand, reduce the solubility of water in a melt (Holloway 1976).

Exsolution of a vapour phase is the necessary consequence of the crystallization of a water-rich melt according to the overall reaction

H_2O-saturated melt → crystals + fluid phase

(Niggli 1920; Burnham 1967; Whitney 1975). Metal partitioning between the melt and fluid phase is dependent on temperature, pressure and melt composition/structure, particularly the activity of complexing agents. The number of controlling variables makes the generalization of specific experimental data and their application to natural systems difficult. There is, however, general agreement that chlorine, the most important metal carrier in aqueous solutions, partitions strongly in favour of the fluid phase (Kilinc and Burnham 1972; Shinohara et al. 1989). A similar behaviour, although less pronounced, is indicated for boron ($D_B$aq/melt ≈ 3; Pichavant 1981; London et al. 1988). Fluorine, on the other hand, partitions preferentially into a granitic melt phase relative to a hydrous fluid phase (Hards 1978; Dingwell 1988; Webster 1990). Such partitioning behaviour implies that a cooling water-saturated silicic melt in a closed system will remove fluorine from the coexisting vapour phase and will strongly enrich the same phase in chlorine and boron.

The loss of the fluxing component boron in a boron-rich melt at water saturation results in rapid crystallization concomitant with accelerated release of a fluid phase, which will amplify explosive phenomena in subvolcanic environments. In addition, explosive vapour exsolution will be enhanced through the irreversible reaction of the boron-rich melt with Fe-Mg-bearing wall rock, i.e. tourmalinization (London 1986).

The partitioning of tin in granitic melt-vapour systems has been investigated with very different results. Nekrasov et al. (1982) and Nekrasov (1984) report data from partition experiments of albite-quartz melt with 13.2 wt% Sn and a fluid phase of variable composition (800°C, 1 kbar, NNO buffer). Their partition coefficients D_{Sn}(fluid/melt) for fluids of various H_2O-HCl-HF-H_3BO_3 compositions scatter widely and are between 0.1 and 0.005 (Nekrasov 1984:97) with a positive correlation of D_{Sn} and chlorine content of the fluid phase. The experiments did probably not attain equilibrium due to low diffusion in the melt (Nekrasov et al. 1982:166) and were possibly hampered by reaction between tin in solution and the container material. In the light of the experiments of Urabe (1985) relatively low partition coefficients for tin may, however, be understandable, taking into account the composition of the synthetic albite-quartz glass charges, i.e. their high alkali/aluminum ratio.

The partitioning experiments by Taylor and Wall (1984) examined the distribution of tin between haplogranite melts and an aqueous chloride-bearing phase with 0-8 m (Na+K)Cl over a range of oxygen fugacities (QFM -1 log unit to HM -1 log unit) at 700-800°C and 1-3 kbar, utilizing a double gold capsule technique. The exact composition of the "haplogranitic" starting

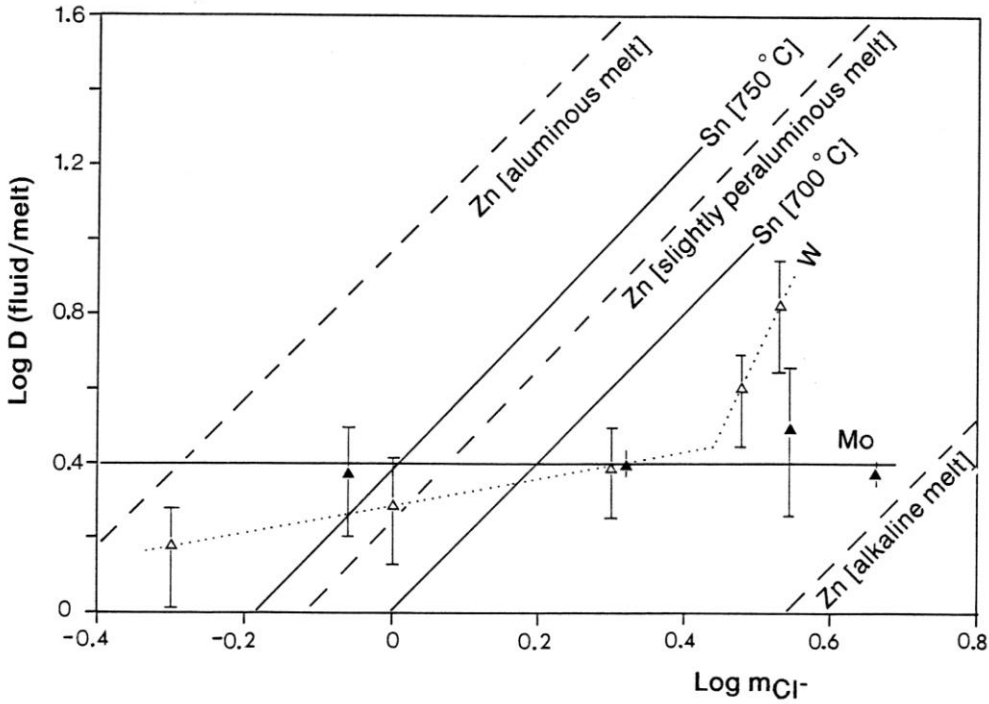

Fig. 12. Vapour-melt partition coefficients for Sn, W, Mo and Zn as a function of chloride molality. Sn data are from experiments by Taylor and Wall (1984), complemented by data in Manning and Pichavant (1988), for 700-800°C, 1-3 kbar, fO_2 fixed but not specified (probably NNO), haplogranitic melt composition. W data (open triangles) from Manning and Henderson (1984) for 800°C, 1 kbar, fO_2 unbuffered, Qz-Ab-Or-H_2O minimum melt. Molybdenum data (solid triangles) from Candela and Holland (1984) for 750°C, 1.4 kbar, melt composition identical to the experiments by Holland (1972), i.e. slightly peraluminous granitic melt. Zinc data from Holland (1972) for 830 ± 20°C, 2.0 ± 0.2 kbar, slightly peraluminous granitic composition, and from Urabe (1985) for 800°C, 3.5 ± 0.25 kbar with both alkaline and aluminous silicic melt

material is not given in Taylor and Wall (1984). Tin was found to partition in favour of the vapour phase. In detail, the partition coefficient varied as a function of oxygen fugacity and of the square of chloride molality, with values of D_{Sn}(fluid/melt) of the order of 1-10. Partition coefficients obtained by Taylor and Wall (given in Manning and Pichavant 1988) are plotted in Fig. 12 in comparison with data for Zn, Mo and W. The zinc partition coefficients are included to underline the fact of the extreme importance of melt composition for such data, with probably the [Na+K+2Ca]/Al ratio of the melt being the most critical parameter (Urabe 1985). D_{Zn}(fluid/melt) increases for two

orders of magnitude from alkaline to aluminous melt conditions. A similar dependence can be expected for tin which, as deduced from the slope in Fig. 12, is predominantly dissolved as a $SnCl_2^0$ complex at magmatic temperatures, analogous to zinc.

The tungsten data in Fig. 12 show a strong preference of tungsten for the fluid phase. The positive correlation of D_W(fluid/melt) with chloride concentration has been interpreted to suggest varying styles of Cl-complexing, in addition to the probable dominance of iso- and hetero-polytungstates at low chloride concentrations (Manning and Henderson 1984). Because the experiments were run with NaCl solutions, this can, however, also be explained as a result of ion pairing of Na^+ with tungstate, which seems more likely in the light of the lack of correlation between W and HCl concentrations in more recent hydrothermal experiments by Wood and Vlassopoulos (1989). The partition coefficient of molybdenum has been shown by Candela and Holland (1984) to be independent of chlorine (and fluorine) concentration in the fluid, which points to the existence of Mo as molybdate species in the aqueous phase.

Taylor and Wall (1984) conclude from their experiments that the tin-carrying capacity of chloride-rich fluids at magmatic temperatures is of the order of 10^2-10^4 ppm Sn. These results are consistent with hydrothermal solubility data of Haselton and d'Angelo (1986), who found approximately 3000 ppm Sn at cassiterite saturation in 1 m chloride solutions coexisting with a synthetic quartz monzonite (700°C, 1 kbar, NNO oxygen buffer). The dependence of tin solubility on temperature, chloride concentration and fO_2 as established for magmatic conditions is confirmed by the hydrothermal solubility studies of cassiterite at submagmatic temperatures (Wilson and Eugster 1984; Eugster and Wilson 1985; Eugster 1986).

2.7 Hydrothermal Solubility of Cassiterite

Tin may be present in aqueous solutions in either the divalent or the tetravalent oxidation state, depending on oxygen fugacity and pH of the system according to the equation:

$$H_2O + Sn^{4+} = Sn^{2+} + \tfrac{1}{2}O_2 + 2H^+. \qquad (23)$$

The solubility of cassiterite in pure water is very low and, with 1 kbar pressure, 500°C temperature and oxygen fugacity defined by NNO reaches only 0.4 ± 0.2 ppm Sn, according to the experimental data from Kovalenko et al. (1986).

Solubility data for lower temperatures and with experimental ***f***O2 conditions not intentionally constrained are slightly lower (Klintsova and Barsukov 1973; Dadze et al. 1981).

Both tin species form aqueous complexes with various ligands, of which Cl^-, F^- and OH^- are the most important in natural hydrothermal fluids (Jackson and Helgeson 1985a). Tin transport via fluoride complexes, first suggested by Daubr,e (1849), seems to be less important because fluoride concentrations in natural hydrothermal solutiuons are restricted by equilibrium constraints involving fluorite, topaz, or other fluoride-bearing minerals with relatively low solubilities (Jackson and Helgeson 1985a).

The solubility of cassiterite in HCl-NaCl solutions has been experimentally studied in the temperature range of 400-600°C and at 1.5 kbar pressure by Wilson and Eugster (1984), Eugster and Wilson (1985) and Eugster (1986). For reducing and moderately oxidized conditions (***f***O2 fixed by NNO buffer) the dissolution and speciation of cassiterite was found to be controlled by the equation

$$SnO_2 + 2H^+ + Cl^- = SnCl^+ + H_2O + ½O_2 \quad (24)$$

with

$$\log K_{24} = 29.3 - (27500/T),$$

where T is in K. Only under strongly oxidized conditions (***f***O_2 fixed by HM buffer) does the tetravalent tin species become dominant in the solution, according to the equation

$$SnO_2 + 4H^+ + 3Cl^- = SnCl_3^+ + 2H_2O \quad (25)$$

with

$$\log K_{25} = 33.2 - (18100/T).$$

Chloride complexes of di- and tetravalent tin species are related by an equilibrium analogous to Eq. (23), i.e. higher Cl^- molality, lower pH and higher ***f***O2 favour tetravalent tin complexes which are, however, important only in very acid solutions throughout the redox stability field of magnetite (Eugster 1986).

If the pH of a solution is buffered by the mineral assemblage K-feldspar-albite-muscovite-quartz (rock-buffered fluid), as is valid for large parts of granitic host rocks of tin deposits, Eq. (24) describes the concentration of the dominant tin complex in a chloride solution. The dramatic dependence of tin concentration on temperature and oxygen fugacity is shown in Fig. 13.

$$SnO_2 + 2H^+ + Cl^- \rightleftharpoons SnCl^+ + H_2O + 1/2O_2$$

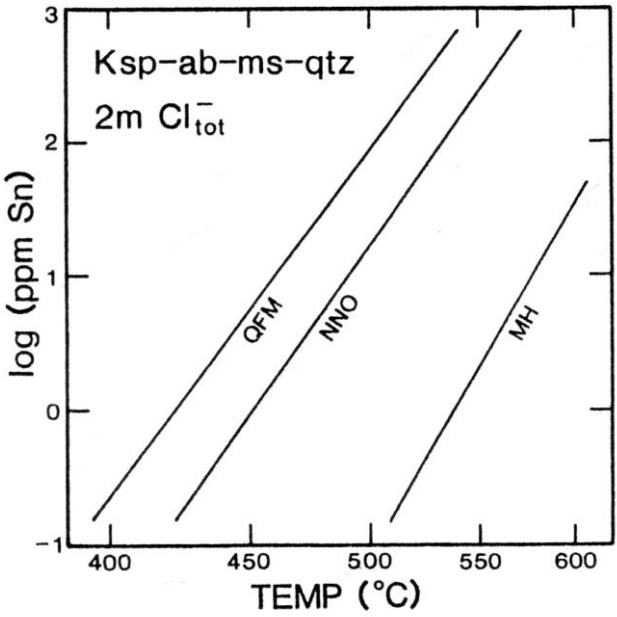

Fig. 13. The solubility of cassiterite in HCl-H_2O solutions as a function of temperature and fO_2 defined by QFM, NNO or MH oxygen buffers. The assemblage K-feldspar + albite + muscovite + quartz defines pH, chloride molality is 2 m (Eugster 1986:666)

A solution at a temperature of 500°C and with stable feldspar will dissolve <1 ppm Sn under conditions of the HM buffer, whereas the same solution under reducing conditions of the QFM buffer is able to transport about 100 ppm Sn. The latter solution will, however, precipitate cassiterite quantitatively in the temperature range 400-450°C. Tin ore formation below about 400°C requires a low-pH fluid (or alternatively: high-pH fluid, less probable in natural environments) not in chemical equilibrium with feldspar, in accordance with the common observation of feldspar-destructive hydrothermal alteration with the mineral assemblage muscovite + quartz ± kaolinite around hydrothermal tin-mineralized veins. The solubility of cassiterite under such acid conditions and in the temperature range of 200-350°C has been calculated by Jackson and Helgeson (1985a,b), taking into account a variety of tin complexes (Fig. 14).

The relatively temperature-independent solubility curve for pH=6 corresponds to the predominance of hydroxide tin complexes with a combined tin concentration around 1 ppm Sn at intermediate pH, in accordance with the experimental data on the SnO_2-H_2O system (Dadze et al. 1981; Klintsova and Barsukov 1973). At lower pH and even with moderate NaCl concentrations in the fluid, Sn^{2+}-chloride complexes are dominant

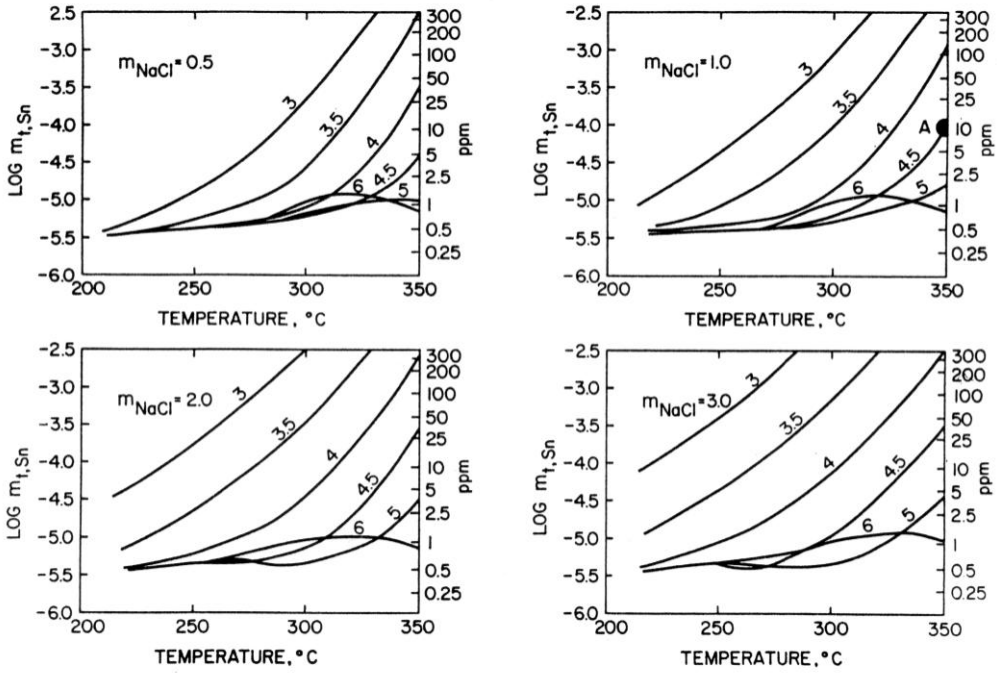

Fig. 14. Solubility of SnO_2 in NaCl solutions in equilibrium with topaz as a function of temperature and pH (numbers on solubility contours). Oxygen fugacity controlled by pyrite-magnetite-pyrrhotite buffer. Pressure along liquid-vapour equilibrium of H_2O (200°C ≈16 bar; 340°C ≈146 bar). Total Sn concentrations include: $Sn(OH)^{3+}$, $Sn(OH)_2^{2+}$, $Sn(OH)_3^{+}$, $Sn(OH)_4^{0}$, $Sn(OH)^{+}$, $Sn(OH)_2^{0}$, $Sn(OH)_3^{-}$, $SnCl^{+}$, $SnCl_2^{0}$, $SnCl_3^{-}$, SnF^{+}, SnF^{0}, SnF_3^{-}. Point A in diagram for mNaCl=1 is an estimate of conditions during early tin ore formation in SE Asian tin belt according to fluid inclusions and mineral association. (Jackson and Helgeson 1985b:1375)

which support tin concentrations in the 100 to 1000 ppm range. Fluoride complexing of tin in such solutions at maximum F- levels allowed by the presence of fluorite or topaz is negligible (Jackson and Helgeson 1985a; Eadington 1988). The steep slope in the diagrams of Fig. 14 points to the importance of temperature control of cassiterite precipitation, which is also dependent on acid neutralization, oxidation and dilution (Cl- concentration). The predominance of hydroxy-tin complexes under alkaline pH conditions is shown in Fig. 15, which indicates a relatively large tin solubility field for pH ≥7 down to moderate temperatures.

Tin ore formation in the epithermal temperature range requires a hydrothermal system partly isolated from mineral buffer assemblages in quartzofeldspathic wall rocks, i.e. a fluid-buffered system (Heinrich and Eadington 1986). This

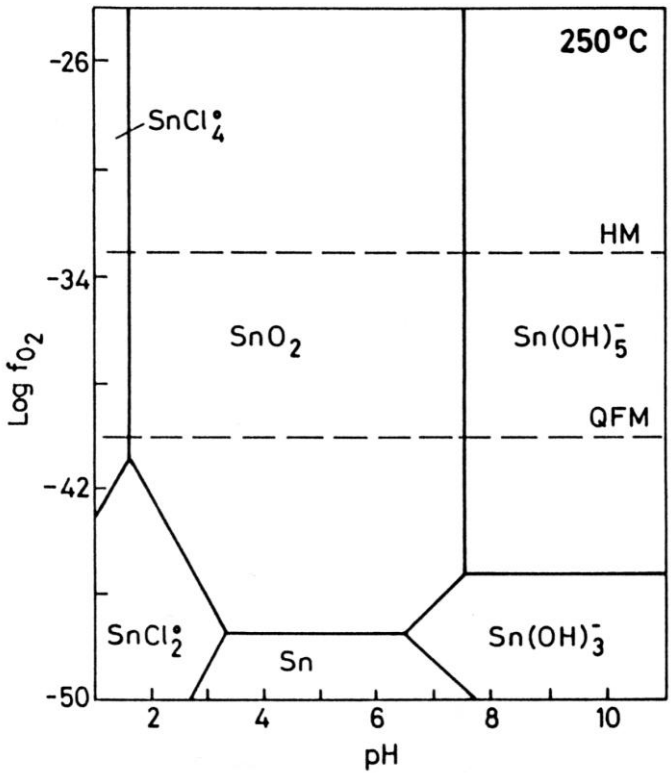

Fig. 15. Equilibrium phase diagram for cassiterite and some chloride and hydroxide complexes of tin at 250°C. Boundaries for the complexes are drawn at an activity of 10^{-3} m, $a_{Cl^-} = 1.0$. If controlled by the solubility of fluorite, a_{F^-} is too low (2×10^{-3}) for fluoride complexes of tin to contribute significantly to the solubility of cassiterite. (Eadington 1988:27)

situation is realized once a halo of completely altered wall rock has formed around fluid channels. Subsequent fluid batches will develop extremely low pH and *f*O2 conditions with falling temperature and cassiterite precipitation [dissociation of HCl plus chemical effects of Eq. (24)]. Modelling by Heinrich and Jaireth (1989) and Heinrich (1990) indicates that a fluid-buffered solution, instead of precipitating cassiterite, may become strongly Sn-undersaturated as it cools. This allows transport of very high tin concentrations (hundreds of ppm) to a low-temperature deposition site, in which finally acid neutralization through wall rock interaction allows cassiterite mineralization.

A little-studied alternative to hydrothermal tin transport by chloride complexing is a colloidal solution process at low salinity. Occurrences of wood tin ($SnO_2 \cdot nH_2O + SiO_2$) suggest a low-temperature formation from metastable, oversaturated solutions which are able to transport polymerized tin compounds in colloidal form and to precipitate cryptocristalline hydrous cassiterite. Wood tin is known from veinlets in volcanic rocks, relics of

colloidal textures are, however, documented also for high-temperature hydrothermal tin deposits (Herzenberg 1936; Lebedev 1967; Seltmann et al. 1985), of which one example is the Chacaltaya district in northern Bolivia (Avila 1982), discussed below.

The hydrothermal solubility of tungsten was recently reviewed and experimentally studied by Wood and Vlassopoulos (1989) under fixed conditions of 500°C and 1 kbar. The average solubility of WO_3 in pure water was around 515 ppm W. Contrasting to the behaviour of tin, no significant increase in solubility was observed in the presence of up to 5 m HCl, implying that chloride complexing of W is not important. WO_3 solubility increased, however, significantly on the addition of NaCl or NaOH, which suggests the importance of a cation-tungstate ion pair such as $NaHWO_4^0$ or polymeric tungsten species. A relatively large scatter for solubility data of WO_3 in low-salinity solutions may be due to the formation of unstable colloids.

The role of chloride seems to be similarly unimportant in the hydrothermal transport of molybdenum. Experimental studies on molybdenite solubility from 200 to 350°C with oxygen and sulfur fugacities fixed by the pyrite-pyrrhotite-magnetite buffer indicate molybdate species to essentielly control Mo transport (Wood et al. 1987). This situation is similar to the partitioning of molybdenum between aqueous vapour and silicate melt, which is unaffected by either chloride or fluoride complexing (Candela and Holland 1984). The hydrothermal mobility of molybdenum in NaCl-KCl-HCl solutions at 300-450°C correlates with oxygen fugacity and pH, i.e. increasing molybdenite solubility with increasing ***f***O2 and increasing pH (Kudrin 1989). This relationship is inverse to the behaviour of tin.

Note on the concept of oxygen fugacity:
Throughout this text ***f***O2 is used as the principal redox parameter. It should be borne in mind that dissolved oxygen is a fictive component in most hydrothermal fluids, which conveniently allows to describe the oxidation state of a geological system. The physical presence of dissolved oxygen is not implied in this concept. A hydrothermal fluid at a temperature of 250°C and with log ***f***O2 -38, i.e. near the pyrite-pyrrhotite-magnetite buffer, has a molality of oxygen of log mO2 -40.6 (Henry's Law constant of 21000), which is 1 molecule of oxygen for each 1016.8 kg of fluid. That is less than 1 molecule per ten thousand cubic kilometres of fluid (see the similar calculation for the BR22 well at Broadlands in Barnes, 1984). Therefore, dissolved oxygen in a reduced hydrothermal environment does not physically exist and has, of course, no role as a redox buffer. Even the much more abundant dissolved hydrogen is a negligible buffer component compared to silicate reactions (Giggenbach 1980).